Stanford Exploration Project, Report 77, November 17, 1997, pages 55–64

Constant-velocity anti-aliasing three-dimensional integral dip moveout

Patrick Blondel[1]

keywords: *amplitudes, DMO, three-dimensional*

ABSTRACT

A method of three-dimensional integral dip moveout processing for constant-velocity media must cope with problems related to amplitude and aliasing. The convolution of the dip moveout operator with triangle functions avoids the aliasing effect. A study of different amplitude weightings leads to the choice of the weighting scheme derived from a Fourier domain expression of dip moveout (Black et al., 1993). Testing the method on a 3-D synthetic data set shows the conservation of the amplitude-versus-offset (AVO) effect throughout the dip moveout (DMO) process.

INTRODUCTION

The Fourier domain DMO methods give appropriate results for 2-D lines but are time-consuming. In 3-D surveys, their implementation becomes more difficult because the spatial sampling rate as a function of azimuth is variable and irregular. In contrast to Fourier domain DMO methods, the integral DMO method is not affected by this problem and provides cheap processing because of the limited extent of the operator (which is two-dimensional and dip-limited). However, the implementation of an integral method requires explicit knowledge of the operator as well as of the weight applied to each operation. The next section describes the shape of the operator, and the second section states three rules that the DMO operator must satisfy.

The shape of the operator

Deregowski (1981) thoroughly described the elliptic DMO operator; I include Figure (1) only for the sake of introducing the terminology used throughout this paper.

[1]**email:** not available

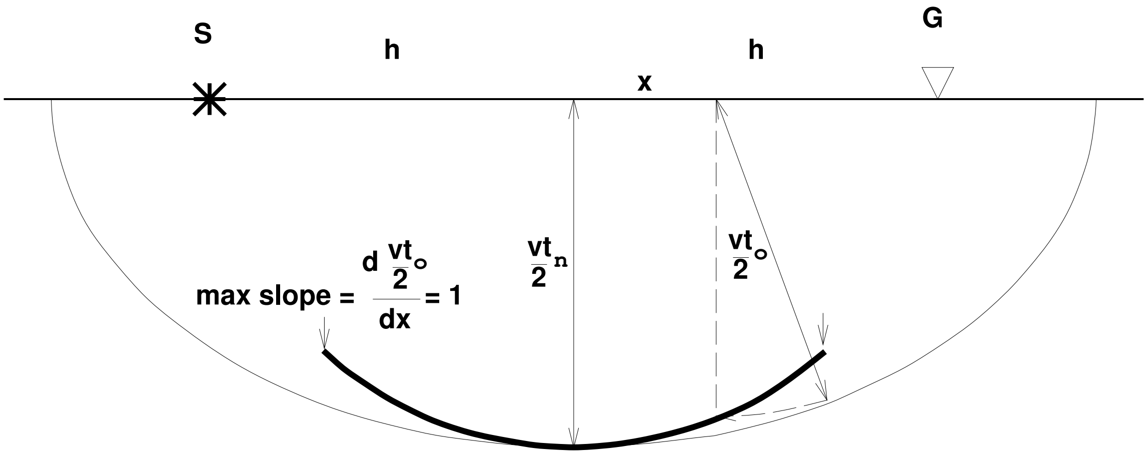

Figure 1: The DMO operator (bold line) is geometrically constructed from the elliptical reflector corresponding to an impulse in a (time, midpoint) section. Notice that in the (t_0, x) space, the maximum slope is $2/v$. patrick1-Shape [NR]

The operator is a dip-limited ellipse whose support is given by the equation

$$\frac{t_0^2}{t_n^2} + \frac{x^2}{h^2} = 1. \tag{1}$$

Because it is kinematically impossible to have reflectors dipping more than the slope $2/v$ in a zero-offset constant-velocity time section, the DMO operator is dip-limited.

The rules the operator must obey

The primary attribute of an integral method is to respect the kinematic component of the process. However, in order to yield a *consistent* stack of the operators illuminating a given location, the integration should be a weighted sum. In other words, an amplitude function should be applied along the operator. The integral DMO process will be *consistent* if it obeys the following rules.

Rule 1. According to Hale (1991), "The impulse responses [obtained by Fourier Transform DMO] may be used as a standard by which to judge integral DMO methods". Because (f, k) DMO methods have a perfect behavior with respect to amplitude, the integral DMO operator should be as close as possible to the (f, k) DMO operator in amplitude and phase. Thus, we expect the integral impulse response to have a low amplitude and a high-frequency content near $x = 0$ and a high amplitude and a low-frequency content when the slope of the operator becomes steeper.

Rule 2. Flat events must not be affected in amplitude and phase by the DMO process. This rule, clearly stated by Hale (1991), is perfectly respected by any (f, k) DMO process (Hale, 1983; Liner, 1990), but it represents a challenging test for integral DMO processes.

Rule 3. Events of a given reflectivity must show balanced amplitude after the DMO process, whatever their dip. This rule is essential in order not to spoil the data for a possible AVO study.

The first section of this paper explains how to avoid the aliasing of the operator. In the next section, the three rules stated above help us choose the most convenient weighting among three amplitude schemes selected from the literature. Finally, a brief section discusses how to apply the operator on a 3-D grid.

THE TRIANGLE AS AN ANTI-ALIASING STRUCTURE

In the Fourier domain, the operator is not aliased. However, integral methods must be applied carefully to account for operator aliasing.

For a given temporal frequency of the data, the increase in the dip of the operator produces an increase in the spatial frequency until it reaches the Nyquist frequency (two points per wavelength). Beyond that point, the operator is aliased.

Claerbout (1992) introduced an efficient technique to avoid the aliasing of the operator with Kirchhoff methods. Instead of spreading a simple spike along the operator, a dip-dependent triangle is effectively convolved with the operator. Assuming spatial spacing of Δx, the width of the triangle at a point of the operator is determined by equation (2)

$$\Delta_t = \left(\frac{dt_0}{dx}\right)\Delta x, \tag{2}$$

where $\left(\frac{dt_0}{dx}\right)$ is the operator dip. It is therefore assured that the operator always has at least two points per wavelength on the spatial axis, even when the time frequency of the data is Nyquist.

Figure (2) shows the impulse response of a spike when the triangle anti-aliasing method is used. The phase shift caused by the half differential filter (usual in Kirchhoff methods) makes the triangles look like the teeth in a shark's jaw.

The triangular weight can be built with three spikes $(-\frac{\Delta_t}{2}, \ldots, \Delta_t, \ldots, -\frac{\Delta_t}{2})$ submitted to both causal and anticausal integration. The anti-aliasing process is cheap because each output trace is double integrated only once.

AMPLITUDES ALONG THE DMO OPERATOR

A rich literature has been published describing "true" DMO amplitudes, which suggests that the truth is variable! In this section, I examine three propositions for amplitude weighting (Beasley and Mobley, 1988; Gardner and Forel, 1990; Black et al., 1993) to find the one that best verifies the rules stated in the introduction. I then discusses the inclusion of factors accounting for the spherical divergence and the effect of anti-aliasing on amplitudes.

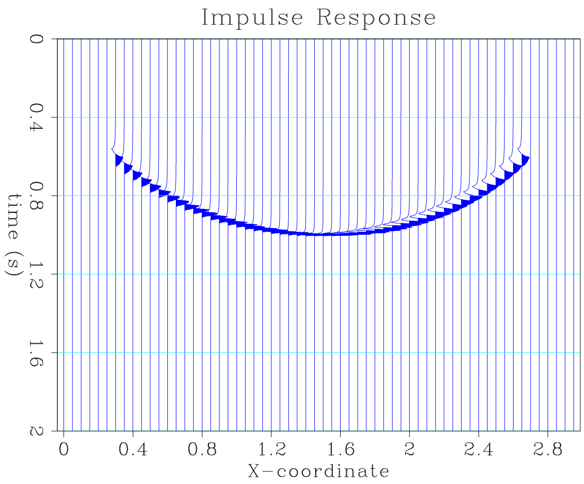

Figure 2: Impulse response of the anti-aliasing integral DMO using triangles. Input spike: 1.0 s; velocity: 2000 ms^{-1}. patrick1-Iraa [ER]

Different weighting schemes

The weighting scheme proposed by Beasley (1988) is based on a heuristic approach. Starting from the dip-domain formulation of DMO (Jakubowicz, 1990), he showed that the amplitudes along the DMO operator are proportional to its curvature $\frac{d^2t_0}{dx^2}$. Then he constrained the amplitudes in time and offset to verify Rule 2, assuming a dominant frequency of the data. He came up with the following expression:

$$A_1(t_n, h, x) = \frac{\Delta x}{\Delta x + 2h\sqrt{2s - s^2}} \frac{1}{\left(1 - \frac{x^2}{h^2}\right)^{\frac{3}{2}}}, \tag{3}$$

where $s = (2f_d t_n)^{-1}$ and f_d is the dominant frequency.

Gardner (1990) introduced the DMO-NMO method and derived a DMO amplitude factor that is directly related to the curvature of the operator through the expression

$$A_2(t_n, h, x) = \left(-\left(\frac{d^2t_0}{dx^2}\right)\right)^{\frac{1}{2}} = \sqrt{t_n}\frac{1}{h}\frac{1}{\left(1 - \frac{x^2}{h^2}\right)^{\frac{3}{4}}}. \tag{4}$$

Recently, Black et al. (1993) derived the following mathematical expression for integral DMO from the (f, k) DMO expression:

$$A_3(t_n, h, x) = \sqrt{t_n}\frac{1}{h}\frac{1 + \frac{x^2}{h^2}}{\left(1 - \frac{x^2}{h^2}\right)^{\frac{3}{4}}}. \tag{5}$$

I now apply the rules to the three weighting schemes and compare their results.

Rule 1. Figure (3) shows the comparison of the different weighting schemes normalized by their value at $x = 0$ with the amplitude picked along the impulse response of an (f, k) DMO program (Zhang's formulation). The different curves agree

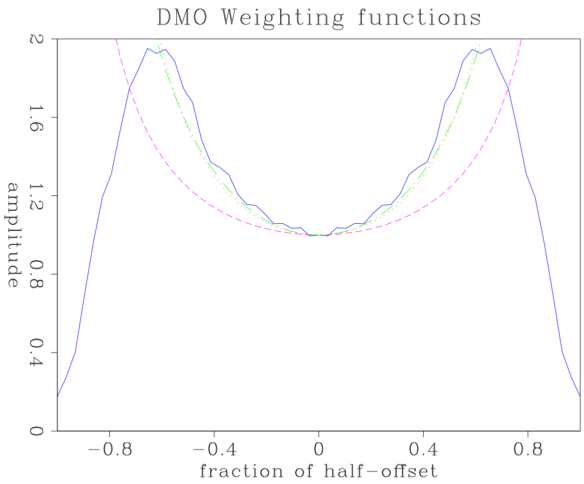

Figure 3: Normalized weighting schemes compared to (f, k) DMO amplitudes. Dotted line: Beasley; Dashed line: Gardner; Dashed-dotted line: Black; Solid line: picked amplitudes on the (f, k) DMO operator. patrick1-Amp [ER]

in shape, their concavity turned upward. However, Black's and Beasley's schemes are closer to the (f, k) DMO amplitudes. The decrease in amplitude of the (f, k) amplitude when x increases is caused by the velocity-dependent dip limitation of the operator. The three weighting functions have been plotted up to $x = h$ without taking the limitation into account.

Rule 2. Figure (4) shows impulse responses that have been stacked along the x-axis. This stack simulates the contribution of impulse responses along a horizontal planar reflector to a single trace. Thus, to obey the second rule, the stacked impulse response should yield the input impulse. The three weighting schemes restore the balanced amplitudes of the impulse rather well. However, Gardner's and Black's schemes show a better stack, especially at earlier times, where Beasley's weighting produces strongest artifacts.

Rule 3. In order to verify the third rule, I used a 3-D synthetic dataset created by David Lumley. Figure (5) shows an NMO-corrected section of the model for a shot located at $x = 0$. The structure is composed of three planar reflectors: a horizontal reflector showing some AVO effect (the amplitudes increase away from the source) and two shallow, dipping reflectors (15 and 30 degrees).

Figure (6) shows the result on the same section after the 3-D DMO. Some strong artifacts appear above the horizontal reflector, and the amplitudes are not well balanced along the reflectors or in relation to each other. This poor result is mainly caused by omission of spherical spreading and the amplitude-boosting effect of the anti-aliasing triangles.

Spherical divergence

As suggested by the preceding result, spherical divergence should be included in the DMO process. Indeed, for a given shot-geophone traveltime, the zero-offset ray path when the reflector is dipping is shorter than when the reflector is horizontal. Since

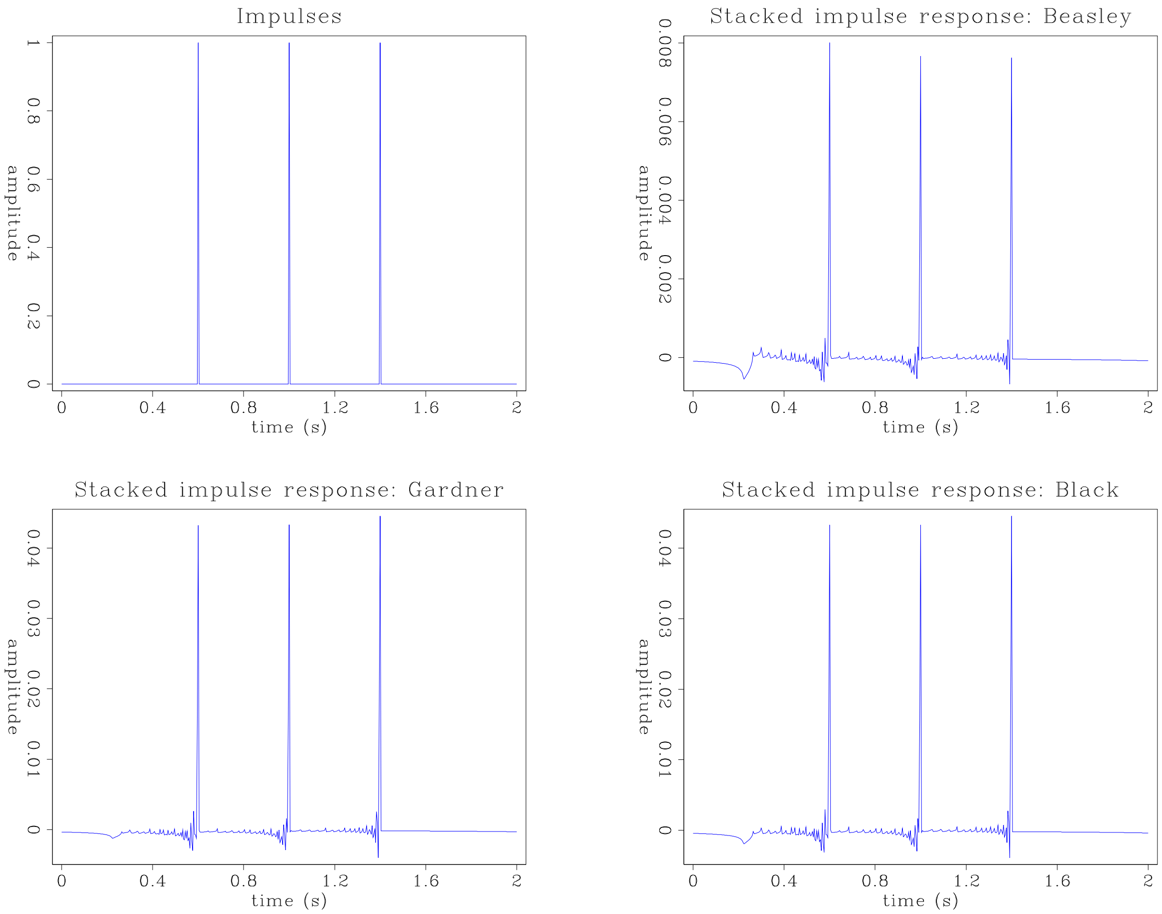

Figure 4: Impulse responses stacked along the x-axis. The top left plot is the input impulse. Three impulse responses have been generated with three weighting schemes and then stacked along the x-axis. patrick1-Imp [ER]

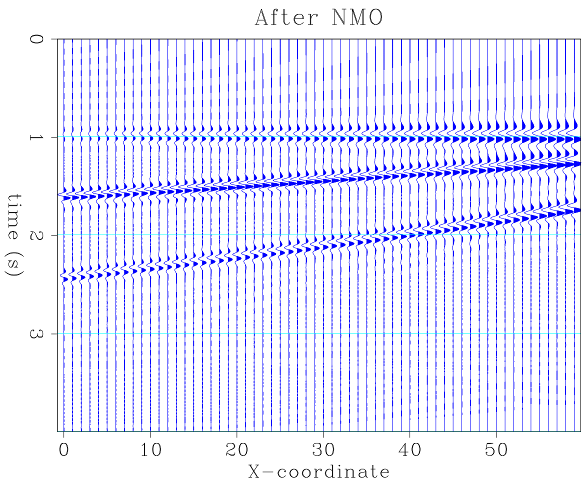

Figure 5: A slice in the 3-D data after NMO. The horizontal plane shows some AVO effect. The two other planes dip at a 15-degree and a 30-degree angle, respectively. patrick1-Nmo [ER]

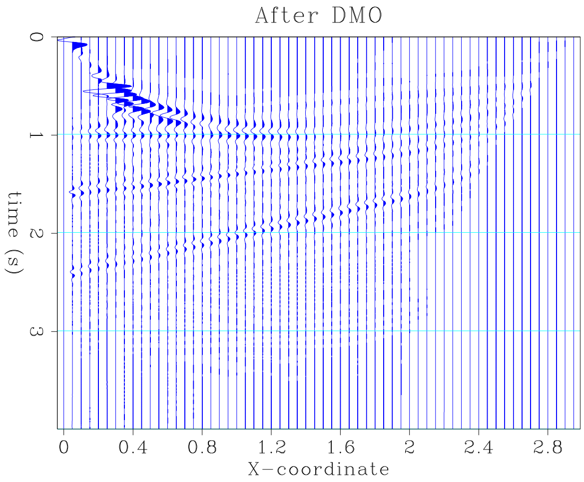

Figure 6: A slice in the 3-D data after DMO with Black's amplitudes, without spherical spreading and without triangle effect corrections. patrick1-Dmo1 [ER]

the decrease in amplitude of a spherical wave is inversely proportional to the distance traveled, the spherical spreading is clearly related to the dip of the structures and, thus, must be included in the DMO process.

Gardner (1990) expressed the spherical spreading factor as a function of k ($\sqrt{h^2 - x^2}$) and t_2 (t_0). As a function of h, t_n, and x, it becomes

$$F_{ss} = h^2 \left(1 + \frac{v^2 t_n^2}{4h^2}\right) \left(1 - \frac{x^2}{h^2}\right). \tag{6}$$

The two first terms of expression (6) account for the offset and the depth of the reflector, whereas the third term clearly accounts for its dip.

The effect of the anti-aliasing triangle width

The anti-aliasing is performed by effectively convolving a triangle function with the output trace. The width of the triangle, Δ_t, usually exceeds the time sampling rate, Δt, for the steepest dips. Therefore, the triangles overlap and produce an undesirable amplitude increase. The number of overlapping triangles is proportional to their width. Thus, a reasonable method of amplitude correction is to divide the convolution triangles by Δ_t, as follows:

$$F_{aa} = \frac{1}{\Delta_t}. \tag{7}$$

Figure (7) shows the same section of the 3-D cube as Figure (6), but the DMO process now involves the two correction factors for spherical spreading and triangle width. The AVO effect along the horizontal reflector is restored, and the relative amplitude of the different reflectors is better balanced and closer to the amplitude distribution in Figure (5). The third rule is now more completely verified although some singularities occur at the near offset traces (close to $x = 0$).

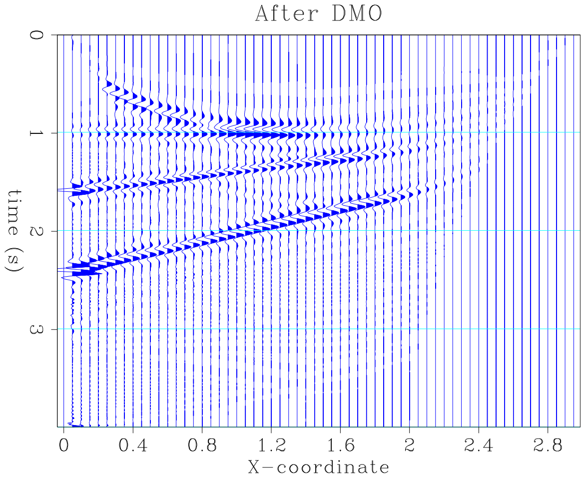

Figure 7: A slice in the 3-D data after DMO with Black's amplitudes, corrected for spherical spreading and the triangle effect. patrick1-Dmo2 [ER]

THE DMO OPERATOR IN THREE DIMENSIONS

As described by Hale (1991), the zero offset rays bouncing off an ellipsoidal reflector of foci S (source) and G (geophone) emerge on the segment $[SG]$. Therefore, the DMO operator is really a 2-D operator working along the source-geophone line, even in a 3-D space. Consequently, applying the operator in three dimensions is not much different than in two dimensions except that the trace smearing is performed for an irregular spatial sampling according to the azimuth. The technique used in this 3-D DMO code consists of computing the bins affected by the segment $[SG]$. More precisely, whenever the center of a bin is closer to the $[SG]$ segment than half the bin size, the bin receives an output trace. This operation is repeated for all input traces, gradually filling the output space. This technique is equivalent to the nearest neighbor interpolation in space and linear interpolation in time described by Nichols (1993).

This algorithm requires some evenly distributed data so that the fold over any bin is nearly constant. Dividing the trace amplitude by the fold of the corresponding bin seems an attractive solution, but it may spoil the AVO properties of the data.

CONCLUSION

I implement a three-dimensional integral dip moveout processing algorithm for constant-velocity media that prevents operator aliasing. The study of amplitudes led me to choose Black's formulation as the most satisfactory in regard to three rules that assure the proper behavior of the DMO process. The method also corrects for spherical spreading.

Although the program has not been tested on real 3-D data, the results with synthetic data, especially regarding AVO restoration, are encouraging. The next step will consist of implementing the algorithm on the Connection Machine.

REFERENCES

Beasley, C. J., and Mobley, E., 1988, Amplitude and antialiasing treatment in $(x-t)$ domain DMO: 58th Annual Internat. Mtg., Soc. Expl. Geophys., Expanded Abstracts, 1113–1116.

Black, J. L., Schleicher, K. L., and Zhang, L., 1993, True amplitude imaging and dip moveout: Geophysics, **58**, 47–66.

Claerbout, J. F., 1992, Anti aliasing: SEP–**73**, 371–390.

Deregowski, S. M., and Rocca, F., 1981, Geometrical optics and wave theory of constant offset sections in layered media: Geophys. Prosp., **29**, no. 3, 374–406.

Gardner, G. H. F., and Forel, D., 1990, Amplitude preservation equations for dip moveout (short note): Geophysics, **55**, no. 4, 485–487.

Hale, I. D., 1983, Dip moveout by Fourier transform: SEP–**36**, 5–34.

Hale, D., 1991, Course notes: Dip moveout processing: Soc. Expl. Geophys., Tulsa.

Jakubowicz, H., 1990, A simple efficient method of dip-moveout correction: Geophys. Prosp., **38**, no. 3, 221–246.

Liner, C., 1990, General theory and comparative anatomy of dip moveout: Geophysics, **55**, no. 5, 595–607.

Nichols, D., 1993, Integration along a line in a sampled space: SEP–**77**, 283–294.